Liquid Crystals
Publication details, including instructions for authors and subscription information:
http://www.informaworld.com/smpp/title~content=t713926090

Local layer structure of the steep field line defect in surface-stabilized ferroelectric liquid crystal cells

Paula C. Willis[a]; Noel A. Clark[a]; Jiu-Zhi Xue[b]; Cyrus R. Safinya[c]
[a] Condensed Matter Laboratory, Department of Physics and Optoelectronic Computing Systems Center, University of Colorado at Boulder, Boulder, Colorado, U.S.A. [b] Department of Physics, Princeton University, Princeton, New Jersey, U.S.A. [c] Corporate Research Laboratories, Exxon Research and Engineering Co., Annandale, New Jersey, U.S.A.

To cite this Article Willis, Paula C. , Clark, Noel A. , Xue, Jiu-Zhi and Safinya, Cyrus R.(1992) 'Local layer structure of the steep field line defect in surface-stabilized ferroelectric liquid crystal cells', Liquid Crystals, 12: 6, 891 — 904
To link to this Article: DOI: 10.1080/02678299208032805
URL: http://dx.doi.org/10.1080/02678299208032805

LIQUID CRYSTALS, 1992, VOL. 12, NO. 6, 891–904

Local layer structure of the steep field line defect in surface-stabilized ferroelectric liquid crystal cells

by PAULA C. WILLIS*, NOEL A. CLARK
Condensed Matter Laboratory,
Department of Physics and
Optoelectronic Computing Systems Center,
University of Colorado at Boulder,
Boulder, Colorado 80309-0390 U.S.A.

JIU-ZHI XUE
Department of Physics, Princeton University,
Princeton, New Jersey 08590, U.S.A.

and CYRUS R. SAFINYA
Corporate Research Laboratories, Exxon Research and Engineering Co.,
Route 22 East, Annandale,
New Jersey 08801, U.S.A.

(Received 31 January 1992; accepted 29 April 1992)

The local layer structure of one type of DC electric field induced line defect observed in CS-1014 surface stabilized ferroelectric liquid crystal electro-optic cells has been determined using X-ray scattering and optical microscopy. The characterized defect is a high contrast defect line distinct from other field lines in that a defect mirror image is not produced when the DC field direction is reversed.

1. Introduction

The surface stabilized ferroelectric liquid crystal device concept [1] is of interest for flat-panel computer and television screens, high speed shutters, optical computing components, and many other applications. In surface stabilized ferroelectric liquid crystal cells, a chevron layer structure frequently occurs when anchored smectic layers shrink in thickness upon cooling, either during cell assembly or upon temperature cycling. This chevron layer structure has been characterized by X-ray and optical studies [2–6]. When a large electric field is applied to many of these chevron cells, line defects form which degrade optical contrast by leaking light in the cell's dark state and blocking light in its bright state. One such line defect is known as the field line, boat wake or roof-top defect, first reported by Dübal [7]. Layer structure changes induced by high electric fields have been reported using X-ray scattering [8, 9]. In this paper we describe field line defects observed in CS-1014 cells and use optical microscopy and X-ray scattering to further develop the previously predicted [8, 10] field line local layer structure.

* Author for correspondence.

0267-8292/92 $3·00 1992 Taylor & Francis Ltd.

The first section of this paper will describe cell construction and optical observations of the two types of field line defects observed, and the theory of the field line formation. We then present our experimental approach and results and finally the structure we have identified for one of the two types.

2. The cell, optical observations and theory

Cells used in these experiments were made of two parallel glass cover slips, 0·16 mm thick, with inner faces coated with indium tin oxide, a transparent electrode, then treated with a rubbed nylon alignment layer, and finally separated by scattered polystyrene beads to make a cell having a liquid crystal layer 1·8 μm thick. The liquid crystal material was Chisso Petrochemical Corporation's CS-1014, with the following phase diagram:

$$C\ -21°C\ S_C^*\ 54°C\ S_A\ 69°C\ N\ 81°C\ I$$

and spontaneous polarization $\mathbf{P} = -5{\cdot}4\,\mathrm{nC\,cm^{-2}}$. The cells were filled, according to standard practice, with the liquid crystal in the isotropic phase, and cooled to the smectic C phase slowly, resulting in the well-understood chevron layer structure discussed later.

Optical observations and photographs were made with Nikon Optiphot-Pol microscope, with the sample between crossed optical polarizers. Microscopically, we have observed that field lines nucleate at spacer beads or the points of a zig-zag wall when an above threshold electric field is applied to the cell. Growth occurs along a line while the field is on, and halts when the field is turned off, resuming where it stopped if the same field is reapplied. Once formed, the defects are permanent, remaining until the cell is thermally cycled through the smectic A, nematic or isotropic phases and re-cooled. For CS-1014 the threshold field for initial defect growth is about $10\,\mathrm{V\,\mu m^{-1}}$. Growth direction depends on chevron directionality (indicated by the zig-zag wall domains) the sign of **P**, and the polarity of the applied electric field **E**. Figure 1 illustrates the two types of field lines, known as the steep and shallow lines, that we examined in this work. Both have similar threshold fields.

In this figure, narrow (lightning) zig-zag domain walls occupy the lower right photo corner, and broad (hairpin) walls are visible in the upper left corner. Zig-zag defects [11] are key evidence of the chevron layer structure. Narrow and broad zig-zag defects mediate a change in chevron direction, and have the bounding chevrons pointing outward or inward, respectively [2, 3, 12].

A steep field line is indicated by the white arrow in figure 1. These field line defects have well-defined boundaries, occur one to a nucleation site, and have long axes roughly 10° from the background layer normal in the cell shown. They never share a nucleation site or occur in mirror symmetric pairs, as the shallow lines often do. In addition, they grow in the general direction of the chevron apex. The background layer normal and the chevron apex directions are indicated in the map inset in figure 1 by the large bold arrow across the layers pointing up and to the left. Shallow field lines, indicated by the black arrow, have more diffuse edges, grow two to a nucleation site in a direction away from the chevron apex, and have long axes around 30° from the background layer normal in the cell shown. The shallow field lines, appearing as inverted V's, have given rise to the boat wake and roof-top defect names.

All near parallel field lines grow under one direction of the applied field. Figure 1 shows a 1·8 μm thick CS-1014 surface stabilized ferroelectric liquid crystal cell in which $\mathbf{P} = -5{\cdot}4\,\mathrm{nC\,cm^{-2}}$. For this cell, an initial applied field of at least 20 V ($E_x < 0$) causes

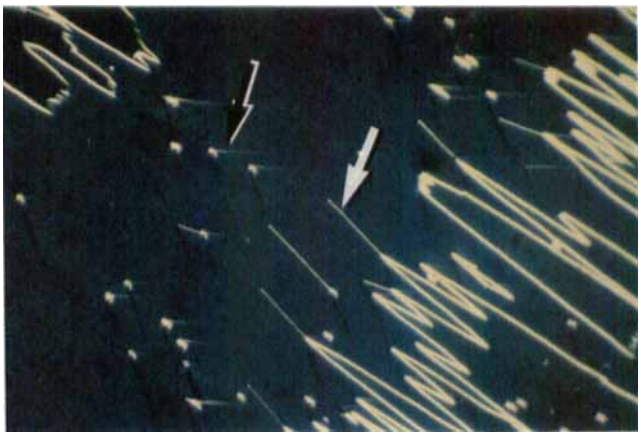

(a)

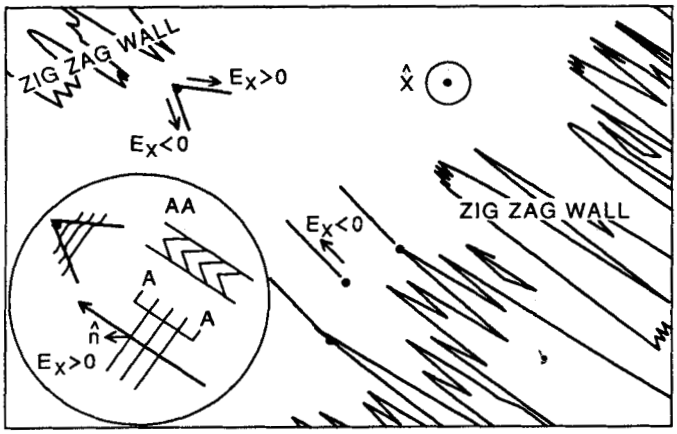

(b)

Figure 1. Steep and shallow field line defects, and electric field effects on director orientation and defect growth. The white arrows point to the steep field line, and the black to the shallow field line defect. The apex of the shallow field line's V is always in the direction of the chevron apex. The vector pointing out of the page defines the convention here for a positive electric field. The large arrow and AA in the inset describe the chevron direction at the figure centre. The inset illustration also shows the general layer connections across a field line defect, and **n**, the director orientation under a positive electric field, $E_x>0$.

growth of steep or shallow field lines, in respectively, the first and third quadrants of a cartesian space referenced to the chevron apex direction. When the field is reversed ($E_x>0$), steep and shallow field lines may grow in the fourth and second quadrants, respectively, from either the original nucleation site or, less commonly, from the newly created field line tip (see figure 2). In general, a steep field line nucleation site does not serve as a nucleation site again. This suggests that nucleation site layer defects are relaxed away by the formation of the steep field line defect much more effectively than for the shallow field line defect, as discussed in § 3.

Mirror symmetry of the shallow lines about a broad zig-zag domain wall is illustrated in figure 3. We have also found that when a sample cell with the line defects is

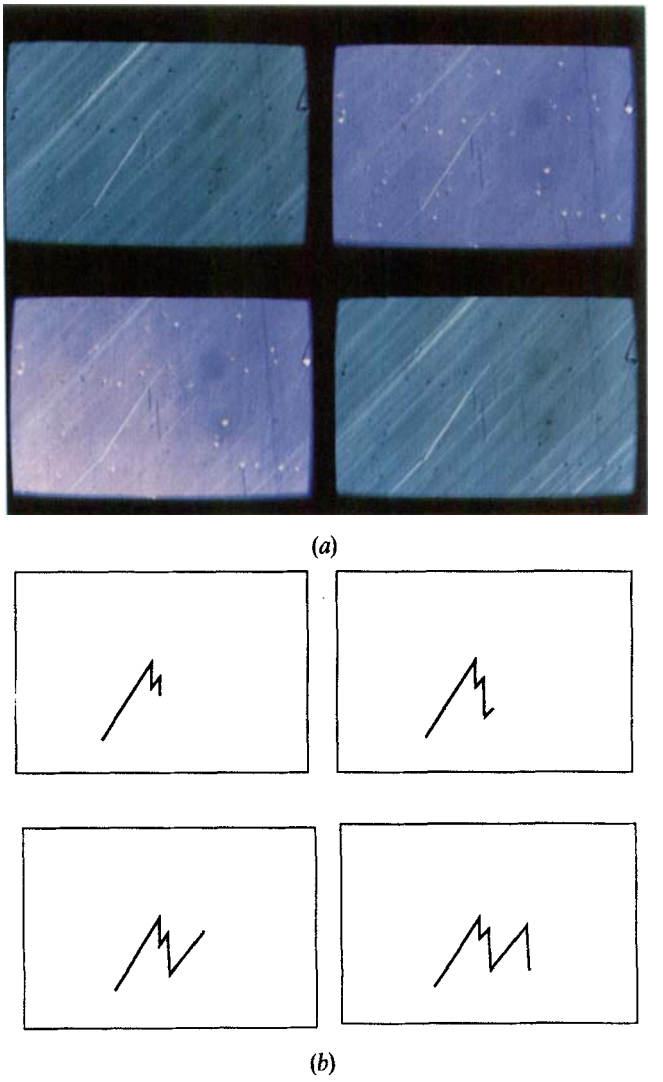

Figure 2. Zig-zag shaped field lines, created by alternating the sign of the applied voltages. The defect is originally nucleated from a polystyrene spacer bead, then the end of the line defect is the nucleation site of the next part when the voltage is reversed.

sheared, replicas of the defects are produced, as shown in figure 4 (*a*). This indicates that the created layer deformation extends completely across the cell and is anchored at both cell walls. When sheared, the two surfaces carry some portion of the distorted regions and hence a replica of the original defect is produced. When sheared back, the original defect and its replica may be superimposed. In contrast, this effect is not observed in the zig-zag defect, which does not alter the layer anchoring at the surface since the defect width converges to a point at the substrate surfaces [2, 3, 13]. Figures 4 (*b*) and (*c*) show field lines in other cells having varying line widths and included angles (cf. § 5).

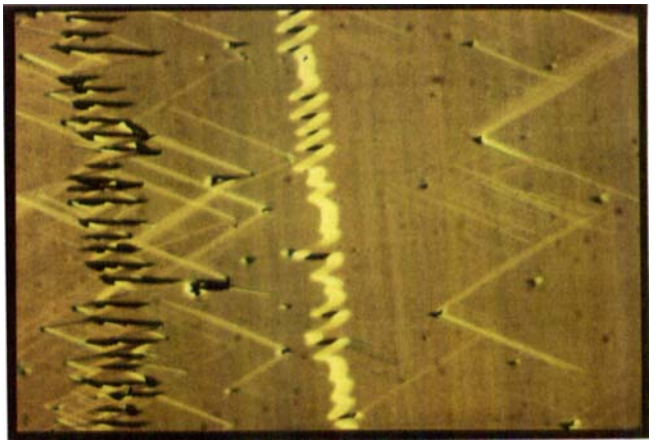

Figure 3. Shallow field line mirror symmetry about the zig-zag defect. A broad zig-zag wall runs across the photo centre. Across a broad zig-zag wall, chevroned layers are symmetric, pointing toward the broad wall.

3. Theory of nucleation and growth

We have observed that most field line nucleation occurs at the tips of zig-zag walls. Three zig-zag tip features favour field line nucleation there: (i) layers within the zig-zag tip are highly kinked, hence vulnerable to degradation; (ii) zig-zag walls contain flattened smectic layers rotated slightly in χ, similar to the field line internal structure, and (iii) they also probably contain high densities of edge dislocations. The last point is drawn from other X-ray scattering experiments [14], which have shown that edge dislocations are present in the surface stabilized ferroelectric liquid crystal cell, and consideration of the chevron formation process, which we expect drives these dislocations into the zig-zag walls.

Under a DC electric field, only one side of the zig-zag wall has a director field well-matched with that of the surrounding chevron [10]. This side of the zig-zag wall possesses the layer orientation favoured for the field line defect, and edge dislocations within that side, especially where the layers are strongly kinked, as in the zig-zag tip, will try to cluster together as they migrate out into the chevron, becoming the field line defect. Our model dictates that the steep or shallow field lines are selected according to the origin and direction of dislocation motion in the zig-zag tip. Dislocation motion which relaxes interlayer tensile stress will be favoured by the large DC electric field that creates the field line defect.

The field line is steep if available edge dislocations originate in the favoured orientation layers, and move from one side of the zig-zag tip directly into the surrounding chevron, without crossing the other, less favoured, side of the zig-zag tip. Shallow field line nucleation appears to combine features of two models. In both, dislocations move away from the boundary between favoured orientation layers and the surrounding chevron. In the first model, the dislocations originate in the favoured layers and move into the less favoured layers. The migrating dislocation breaks up as it goes across the less favoured side of the zig-zag tip, especially in the broad section of the zig-zag wall, making the shallow field line edges fuzzy. This model successfully explains the nucleation site preference for zig-zag tips (due to the probable high dislocation density at the tip centre) and the frequently observed graded fuzziness in the shallow

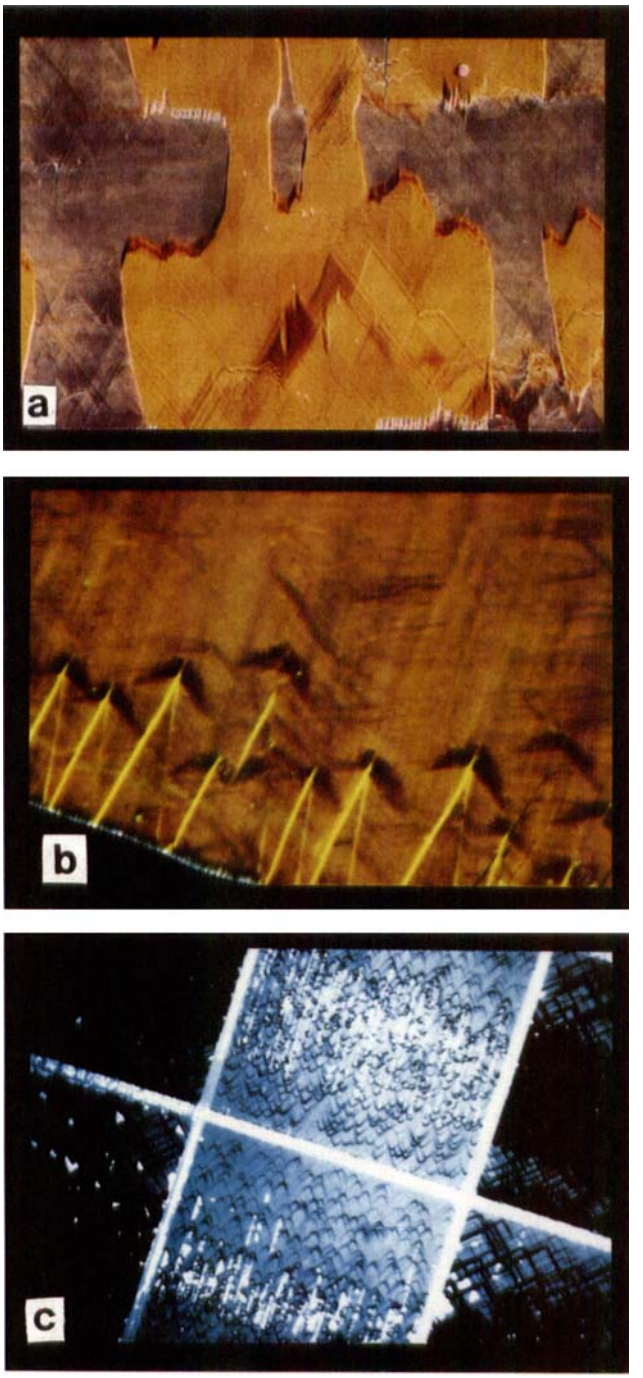

Figure 4. (*a*) Shearing the cell creates replicas of the field line defects, while leaving zig-zag walls unduplicated. (*b*) and (*c*) Field lines in test display cells illustrate the modelled increase of field line half-angle α with line thickness w. The defects in (*b*) are exceptionally wide and also have an exceptionally large half-angle α.

line, while failing to predict the field line angle α. In the second model, the field line grows directly from layer edge dislocations existing at the outer edge of the zig-zag tip, and continuous layer connectivity at the boundary determines the shallow field line angle. This model predicts the field line angle of growth, but does not explain the limitation of nucleation sites to the zig-zag tip. More details will appear elsewhere [15].

Regarding the field line defect's growth, a chevroned surface stabilized ferroelectric liquid crystal cell has at least a two step response to any applied field **E**. In the first response, at low applied fields, the molecules progressively rotate about their individual imaginary tilt cones [14]. This reduces the angle between **P** and **E** to about δ, the layer tilt angle. The second phase is layer deformation, which more completely aligns **P** and **E**.

We envisage the details of the field line growth as follows: the molecular long axis orientation in indicated by **n**. Motion of **n** is in general limited to the imaginary tilt cone such that **n** always maintains an angle ψ about the local layer normal, where ψ is 22° for CS-1014 at room temperature. **P**, the molecular polarization, is at right angles to both **n** and the local layer normal. With no applied field, **P** is uniform from one substrate to the chevron interface, **n** being parallel to the substrate, and splayed from the chevron interface to the other substrate [3, 5]. Under a low electric filed **E**, the driven rotation of **n** about the tilt cone reduces the static ferroelectric free energy $-\mathbf{P}\cdot\mathbf{E}$. Within the surface stabilized ferroelectric liquid crystal chevron, splay of the director and polarization fields is compressed, with the chevron structure remaining undisturbed, and the director and polarization fields approaching a locally uniform alignment within the bent layers. Again, up to this point changes in the initial chevron configuration are extremely small, whether by flattening or by any other structural shift.

As **E** continues to increase, its interaction with **P** results in a torque τ, on the chevroned layers (see figure 5)

$$\tau = \int (\mathbf{P}+\mathbf{E})\cdot d\mathbf{r}, \tag{1}$$

with **r** along **x** and the integral taken across the cell. The torque forces **P** and therefore the layers to be more perpendicular to the cell walls. This change increases interlayer

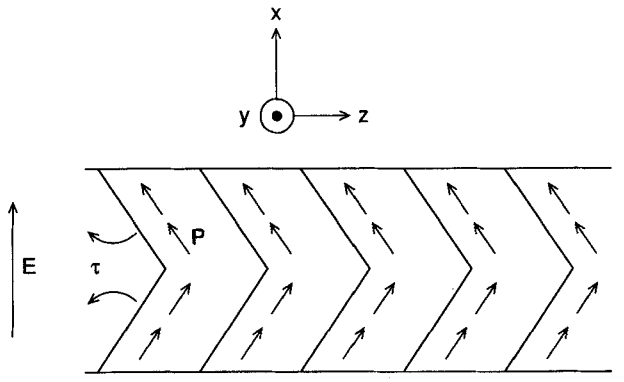

Figure 5. Molecular polarization directions, **P**, and applied electric field, **E**, couple to affect a torque on the chevroned smectic layers.

spacing and is strongly resisted by interlayer tensile stress. If the applied field is increased, surface anchoring eventually fails and the layers reorient, locally rotating in χ, in order that the smectic layers may be continuously connected. The linear progression of this local reformation forms the field line defect.

The induced layer rotations both re-establish continuous layer connectivity as well as balancing the energetically costly induced director splay with the electrostatic applied field energy $-\mathbf{P}\cdot\mathbf{E}$ across the field line under the applied high field when the defect is created. When subjected to a high electric field and viewed in a polarizing microscope, the extinction direction and optical transmission of the active field lines and the background chevroned areas become indistinguishable, indicating that the director fields of the background chevron and the active field line interior are very similar (for a plot of extinction angle versus voltage, see figure 2 in [16]). Active field line defects are those most likely to undergo growth under an applied field of a given polarity. This director reorientation match is visible microscopically via the markedly reduced contrast of the active field lines against the unchanged background, at any cell orientation, for applied fields **E** approaching threshold.

4. X-ray scattering: experimental approach and results

The X-ray scattering was carried out at Brookhaven National Laboratory's National Synchrotron Light Source, using the Exxon X-10B beam line. A bent Ge crystal acting as monochromator selected the Cu–K_α wavelength of 1·54 Å used in our diffraction experiments. Sample and detector were oriented about (χ, β) and (2θ) axes, respectively, using a four circle Huber diffractometer (see figure 6). In the ideal S_A phase the scattering peak appears at $\chi=\beta=0$, and in the ideal S_C chevron structure, at $\chi=0$ and $\beta=\delta_{1,2}$, where $\delta_{1,2}=\pm\delta$ are the chevron layer tilt angles. In CS-1014 near room temperature, $\delta=19°$. The χ rotation axis is perpendicular to the cell surface and, initially, to the incoming beam. The β axis is parallel to the cell surface, horizontal, and perpendicular to the incoming beam. The 2θ axis is parallel to the β axis. The cell is initially oriented with the S_A layer normal direction vertical and perpendicular to both the β and χ axes.

Scattering measurements were made on the sample both before and after inducing the field lines. A representative run appears in figure 7. Field lines for these runs were induced with +40 V applied for one minute, with polarity determined according to the convention of figure 1. Only the steep field lines were present in the sampled volume, occupying a few per cent of the tested volume. All field lines were parallel and have been grown under one electric field polarity.

The scattering from this sample showed two major changes. Firstly, low level signal appeared between the major chevron peaks and is believed to be diffraction from the field line defect. Second, the main chevron peaks moved slightly toward one another in β without a matching change in 2Θ, due to motion of dislocations present in the bulk chevron. A rise in inter-peak signal due to a combination of these two effects is shown in figure 8.

4.1. *Steep field line signature*

Concerning the first change, a low, irregular ridge, with intensity about 2·5 times background, appears between the two main chevron peaks. This low ridge has two small diffraction peaks (10 times background) at $(\chi,\beta)=(\gamma_1,\delta'_1)$ and (γ_2,δ'_2), where $(\gamma,\delta')_{1,2}\equiv(-7°,-5°),(-7{\cdot}5°,7{\cdot}5°)$. The original large chevron scattering peaks were at $(\chi,\beta)=(0,\pm\delta)\equiv(0,\pm19°)$ (see figures 7 (*a*) and (*b*)).

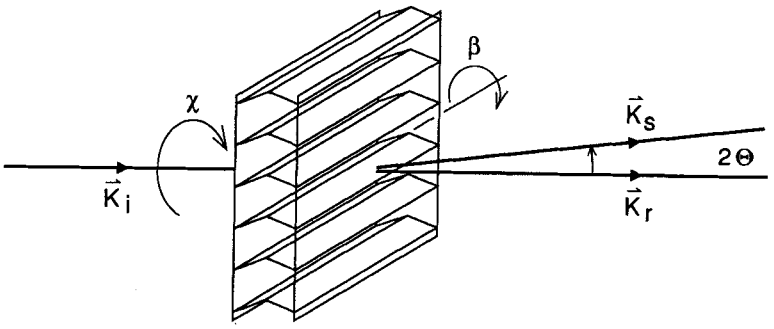

Figure 6. The X-ray scattering configuration.

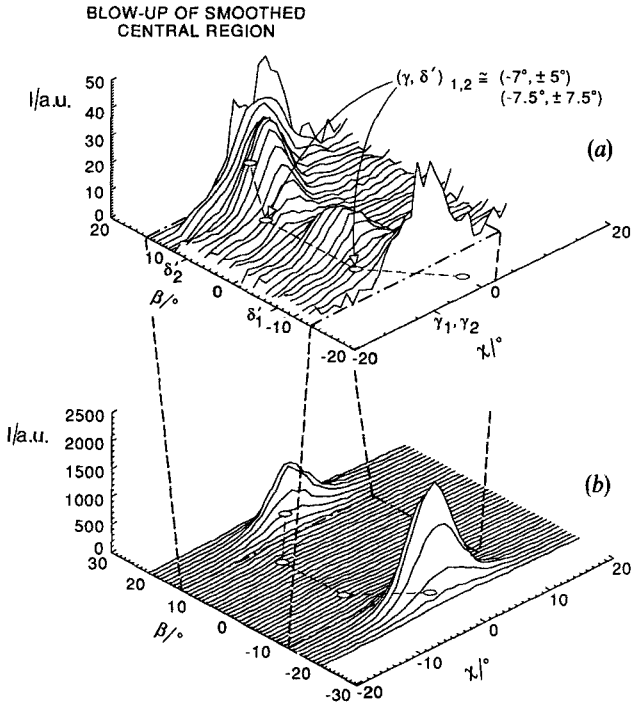

Figure 7. A representative scan in (χ, β) after inducing the field line defect. 40 V has been applied across the cell, as described in the text, to induce the field line defects. (*a*) The new signal appearing in the scan. The two new peaks' apex positions in (χ, β) are defined as $(\gamma, \delta')_{1,2}$. The illustrated data has been smoothed for clarity. (*b*) The complete scan, in which the two original chevron peaks are most conspicuous, and the new ridge is visible as noise between them.

The two small new peaks shown in figure 7 (*b*) are reminiscent of the original chevron pattern having peaks at $(0, \pm\delta)$, with the two peaks $(\gamma, \delta')_{1,2}$ suggesting the field line is a flattened chevron layer structure rotated in χ. This is consistent with our optical observations as discussed previously.

However, a ridge of scattering continuously connects the $(0, \delta)_{1(2)}$ peak with $(\gamma, \delta')_{1(2)}$, its nearest new neighbour. The ridge line in (χ, β) (see figure 9 (*a*)) follows the

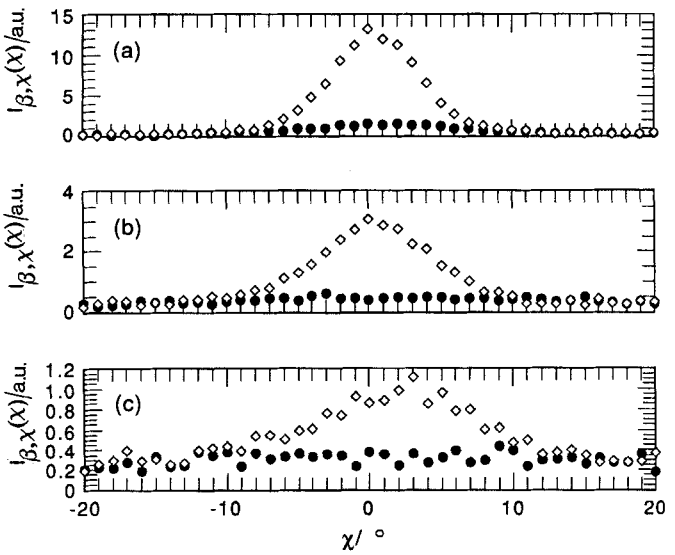

Figure 8. X-ray scattering intensity distribution versus χ before (●) and after (◇) inducing the field line defect, showing the appearance of the ridge at orientations (*a*) $\beta = 14{\cdot}5°$, (*b*) $\beta = 12{\cdot}5°$, and (*c*) $\beta = 10{\cdot}5°$.

path expected for reflections from a cylinder formed by displacing a line common to both the original and tilted chevron layers. This suggests that the chevrons within and without the field line are smoothly connected. $\beta = 0$ divides signals from the upper and lower halves of the chevron (see figure 9 (*b*)).

The ridge extending from one large peak to the other appeared only for $\chi < 0$ for the case of positive applied voltage, i.e. with only one of the two sides of a field line generated. Negative applied voltage generated the other sides of both the field line and the ridge in the X-ray scattering pattern; the other side of the field line is a mirror image of the first, symmetric about a line parallel to the layer normal. The other side of the diffraction pattern is another ridge appearing in the $\chi > 0$ half space. $(\gamma, \delta')_{1,2}$ define the new peak positions in (χ, β), indicated by the arrows in figure 7 (*a*). With both signs of electric field applied to the test cell, both sides of the field lines appeared and two ridges in χ appeared, symmetric about $\chi = 0$. Scattering into these low, peaked ridges appears to be due to the newly created steep field lines.

4.2. *Background chevron scattering*

Concerning the second change, the original chevron peak separation decreased by about 2·6° in β, and 2Θ decreased by 0·006°, immediately after formation of the field line defect. The separation of the large peaks in β has been shown [3, 4] to be the angular separation of the upper and lower chevron. The shift in 2Θ and one fourth of the shift in β appear due to a 0·5°C rise in experimental chamber temperature.

The remaining β peak shift can only be due to chevron flattening by layer edge dislocation motion, which maintains a constant interlayer distance. We know that layer edge dislocations are present in the initial chevroned cell from a comparison of the width of diffractive peaks in β to the width of the 2Θ peak [14]: the initial peaks in β are broader than we expect based on the resolution of the 2Θ peaks. The dislocations in the smectic layers which broaden β are parallel to the layers and the substrate surface.

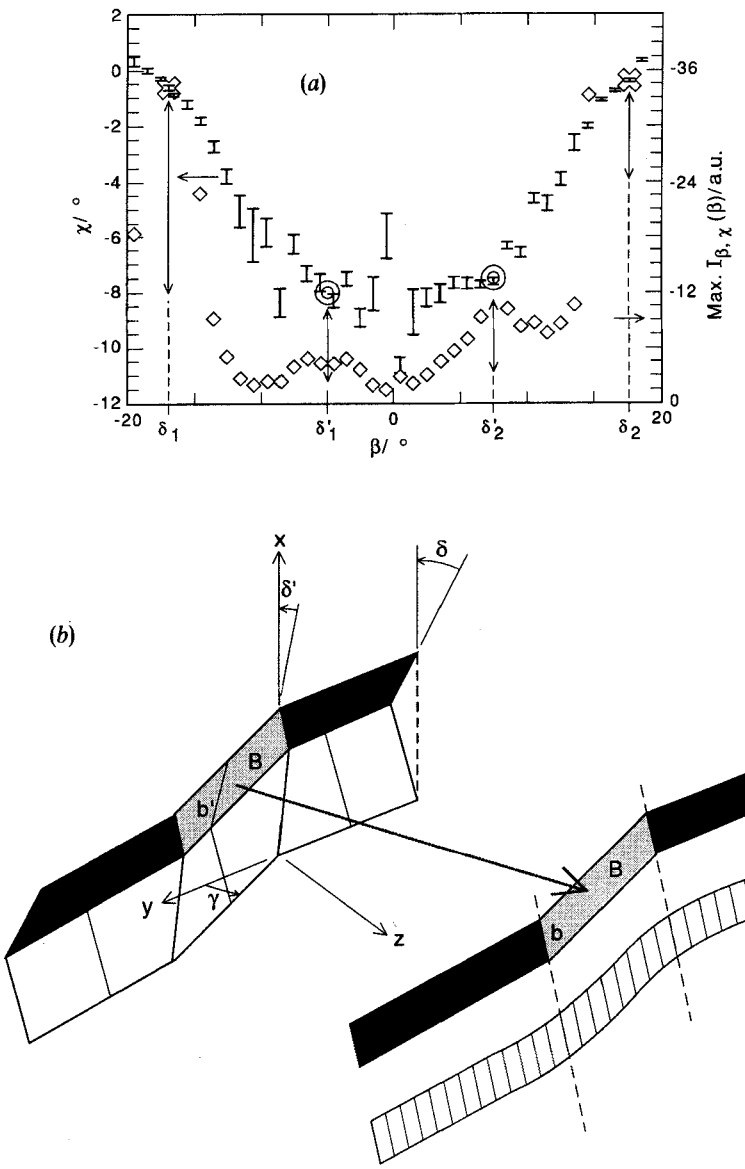

Figure 9. (*a*) Path of the ridge crest in (χ, β) appearing after the defect onset. The ridge lies along two straight lines $\delta'_i < |\beta| < \delta_i$, $i = 1, 2$. The error bars indicate peak positions in β and half widths of gaussian curves fitted to the $I_{\beta,\chi}(\chi)$ distributions. Matched widths increase as peak height decreases due to a non-zero noise level. Intensity versus β is indicated by ◇. (*b*) A cylinder produces a straight line of scattering. Here the intersection line, b, of planes A and B follows a cylindrical surface, smoothing the joints between the internal and external chevrons across the field line, as shown in the hatched area. Planes A and C are parallel. Lines a', b', and c' are lines of steepest gradient in planes A, B and C, respectively.

When an above threshold field is applied to the cell, these dislocations move, relieving the interlayer stresses created by electric field induced layer flattening.

5. Geometrical considerations

The proposed structure and its relation to the various X-ray and optical features is shown in figure 10. The idealized field line geometry is completely described [10] by the angles δ, α, γ, δ' and width w, which are related by

$$\sin\alpha\left(\tan\delta-\frac{\tan\delta'}{\cos\gamma}\right)=2x\left(\frac{\cos\delta'\cos\gamma}{\cos\delta}-1\right), \tag{2}$$

and

$$\frac{\cos\alpha}{\cos(\alpha+\gamma)}=\frac{\cos\delta'}{\cos\delta}, \tag{3}$$

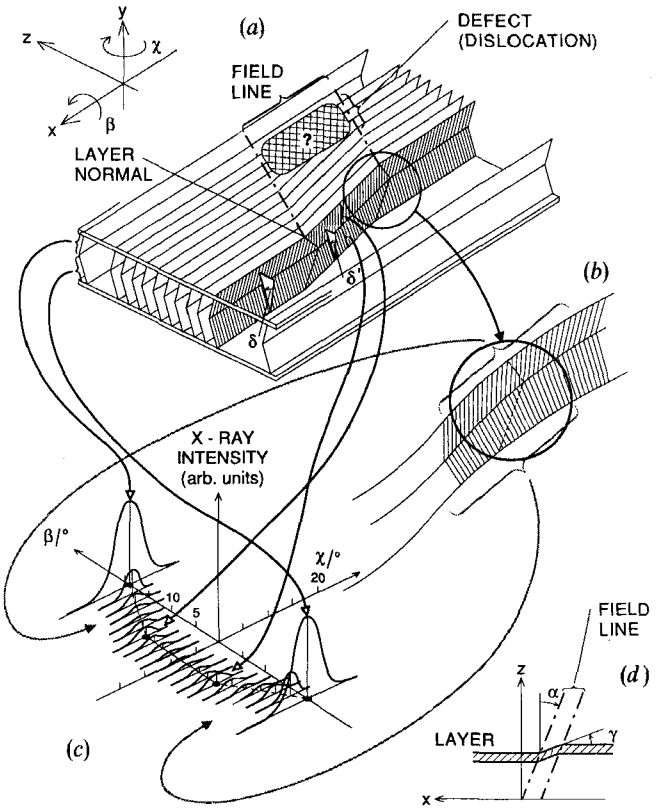

Figure 10. The field line defect and related observations. (*a*) The basic defect structure. $\delta' < \delta$, where δ' is the chevron angle within the field line, and δ is the chevron angle outside the field line defect. (*b*) The layers are smoothly connected across the defect. (*c*) $(\gamma, \delta')_{1,2}=(-7°, -5°)$, $(-7{\cdot}5°, 7{\cdot}5)$ and $(0, \delta)_{1,2}=(0, \pm 19°)$, the small and large peak positions in (χ, β), indicate the layer orientations for chevroned layers within the field line and in the background, respectively. The ridges connecting peaks in the same quadrant are evidence of smooth layer connections. (*d*) γ is the extremum of the layer rotation in χ within the field line, and α is the angle between the S_A layer normal and the field line's long axis.

where α is the angle between the smectic A layer normal and the field line, γ is the most extreme layer tilt about the axis **x** within the field line, δ is the undisturbed chevron layer tilt from the smectic A orientation about **y**, δ' is the chevron layer tilt within the field line, and x is the ratio of the defect line width w to the sample thickness t, $x \equiv w/t$. We expect x to be about 1, since the width of the line defect in the steep field line should be the same as the dislocation core size, which should be comparable to the sample thickness. This is consistent with optical observations, generally to within a factor of 3. The growing end of the steep field line is effectively a giant edge dislocation, with a Burger's vector of approximately 1000 within a single field line tip.

Equations (2) and (3) predict that α will increase with x, given a constant δ and δ', consistent with the generally observed trend: the shallower lines (largest α) are the broadest (see figure 1, 4(*b*),(*c*)). With $x=1$ and δ, δ' fixed at the measured values of $\delta = 19°$ and $\delta' = 7{\cdot}5°$, we calculate $\alpha = 26°$ and $\gamma = -5°$. Optically, we measure $x \sim 1$, but $\alpha \sim 10°$ to $15°$ for sharp lines and $30°$ for shallow lines, and with X-ray scattering, we have $\gamma = -7{\cdot}5°$ when $\delta' = 7{\cdot}5°$. Using $x = 0{\cdot}7$, we calculate $\alpha = 15°$ and $\gamma = -8°$, values which well-match the experimental measurements for sharp field lines. The discrepancy between the calculated and measured values is probably due to the difficulty of estimating field line core size. Because the layers appear to be smoothly connected between the defect interior and exteriors, optical measurements in general overestimate field line width w, and hence x.

6. Conclusion

To summarize, we have identified the local layer structure of the field line defect as a narrow diagonal zone of flattened chevron layers rotated by γ in χ (see figure 10(*a*)). The layer connections across the field line are smooth (see figure 10(*b*)), and (γ, δ'), the extrema of layer angular offsets in (χ, β), are given by the peak positions of the small new signal, in this case $(\gamma, \delta')_1 = (-7°, -5°)$ and $(\gamma, \delta')_2 = (-7{\cdot}5°, 7{\cdot}5°)$ (see figure 10(*c*)). This is consistent with optically observed extinction directions across field line defects (see figure 10(*d*)).

Future work is needed on the details of the following. Firstly, the details of shallow defect formation are still under debate. Second, there is the remarkable consistency in the angle α for a given type of field line. Note that equations (2) and (3) do not uniquely define the field line parameters. Thus there may be some unconfirmed interaction establishing α.

The X-ray experiments reported here were carried out on the Exxon beam line X10-B at the National Synchrotron Light Source at the Brookhaven National Laboratory, which is supported by the U.S. Department of Energy. The authors would like to acknowledge the able technical support of Steve Bennett at Exxon's NSLS beam lines, and the illustrative labours of Dennis Ehmson. This work is supported by NSF Solid State Chemistry grant number DMR 8901657, ARO Center DAAL 03 90-G-0002 and the Optoelectronic Systems Center by NSF Engineering Research Center grant number ECD 9015128 and by the Colorado Advanced Technology Institute (CATI), an agency of the State of Colorado.

References

[1] CLARK, N. A., and LAGERWALL, S. T., 1980, *Appl Phys. Lett.*, **36**, 899.
[2] CLARK, N. A., and RIEKER, T. P., 1988, *Phys. Rev.* A, **37**, 1053.
[3] CLARK, N. A., RIEKER, T. P., and MACLENNAN, J. E., 1988, *Ferroelectrics*, **85**, 79.

[4] RIEKER, T. P., CLARK, N. A., SMITH, G. S., PARMAR, D. S., SIROTA, E. B., and SAFINYA, C. R., 1987, *Phys. Rev. Lett.*, **59**, 2658.
[5] MACLENNAN, J. E., CLARK, N. A., HANDSCHY, M. A., and MEADOWS, M. R., 1990, *Liq. Crystals*, **7**, 753.
[6] MACLENNAN, J. E., HANDSCHY, M. A., and CLARK, N. A., 1990, *Liq. Crystals*, **7**, 787.
[7] DÜBAL, H. R., ESCHER, C., and OHLENDORF, D., 1988, *12th International Liquid Crystal Conference*, Freiburg, Germany (post-deadline paper).
[8] XUE, J.-Z., CLARK, N. A., and WILLIS, P. C., 1989, *Bull. Am. Phys. Soc., APS March Meeting*, Anaheim, California, U.S.A.
[9] WILLIS, P. C., and CLARK, N. A., 1990, *Digest of Technical Papers, 1990 International Symposium of the Society for Information Display*, **21**, 114, Las Vegas, Nevada, U.S.A.
[10] XUE, J.-Z., 1989, Ph.D. Thesis, University of Colorado at Boulder.
[11] HANDSCHY, M. A., CLARK, N. A., and LAGERWALL, S. T., 1984, *Ferroelectrics*, **59**, 69.
[12] OUCHI, Y., TAKANO, H., TAKEZOE, H., and FUKUDA, A., 1988, *Jap. J. appl. Phys.*, **27**, 1.
[13] CLARK, N. A., and LAGERWALL, S. T., 1991, *Ferroelectric Liquid Crystals: Principles, Properties and Applications* (Gordon & Breach), p. 53.
[14] WILLIS, P. C., CLARK, N. A., and SAFINYA, C. R., 1992, *Liq. Crystals*, **11**, 581.
[15] WILLIS, P. C., 1992, Ph.D. Thesis, University of Colorado at Boulder (submitted).
[16] HARTMANN, W. J. A. M., VERTOGEN, G., GERRITSMA, C. J., SPRANG, H. A. v., and VERHULST, A. G. H., 1989, *Europhysics Lett.*, **10**, 657.